PERGAMON

Journal of Structural Geology 23 (2001) 165–182

JOURNAL OF STRUCTURAL GEOLOGY

www.elsevier.nl/locate/jstrugeo

Fracture and surface crust development in a Holocene pahoehoe lava flow on the Island of Tenerife, Canaries

M. Dance, P.L. Hancock[1], R.S.J. Sparks*, A. Wallman

Department of Earth Sciences, Wills Memorial Building, Bristol University, Queens Road, Bristol BS8 1RJ, UK

Received 31 January 2000; accepted 23 June 2000

Abstract

An almost horizontal pahoehoe surface in a Holocene plagioclase basanite lava on Tenerife displays three scales of fracture within the surface crust. An early-formed set of large-scale fractures divides up the surface into an orthogonal set of rectangular slabs with dimensions of several metres and depths of 10–12 cm. The shortest slab dimension is parallel to the flow emplacement direction, inferred from a strong surface lineation. The slabs are domed with the centre an average of 9.6 cm (with range 4–19.6 cm) above the edges of the slabs. Profiles of the slabs normal and perpendicular to the margins and through the crest indicate that they can be described by a power law in which the deflection of the slab, h, is related to the distance from the crest, x, with an exponent between 2 and 3. Analysis of joints within the slabs indicates two smaller scale networks. An intermediate scale joint network bounds blocks with rectilinear to polygonal shapes in plan-view and has a characteristic mean spacing of 24.2 cm (range 10.5–48 cm). The major fractures in this set are normal and parallel to the slab margins. A smaller-scale joint network bounds polygonal equant blocks in plan-view and has characteristic spacing of 6.4 cm (range 3.7–10.5 cm). A model of cooling from the pahoehoe surface is used to constrain the growth of the crust and timing of fracture development. The large-scale slabs are attributed to localised accumulation of gas beneath the growing crust causing buoyant forces. The tensile stresses caused by uplift are sufficient to form the large-scale fractures after 2 or 3 h of cooling. The intermediate scale fracture network is attributed to the flexure of the slab crust. The smaller scale polygonal joint network is related to the build up of isotropic tensile stresses in the cooling slab crust due to thermal contraction with fracture development being promoted by the flexure of the slabs. An analysis of the slab deformation indicates that lava crust is weak. The weakness is explained by division of the crust into three zones: an outer zone with small scale joints that cause negligible strength, a middle zone of elastic behaviour in which stress can build up, and a lower zone of plastic deformation. The crustal slabs display profiles similar to that expected in a bending elastic plate. The deformation of the 10-cm-thick crust can be explained if the elastic zone was about 2-cm thick. This result agrees with an independent calculation of elastic zone thickness based on the position of the brittle–ductile transition being located at the 600°C isotherm at a depth of about 2 cm when the crustal slabs were rifted apart.

1. Introduction

An important aspect of lava flows is the development of a cooled crust. Lava movement is inhibited by crustal growth and so understanding its physical properties and deformation behaviour are important topics in volcanology. Fracturing of lava crust is usually attributed to thermal contraction, generating tensile stresses, and shear stresses related to flow. Other possible causes of crustal deformation are residual motions of the lava interior due to slow inflation, convection and localised accumulation of gas beneath the crust after emplacement. A first-step towards understanding fracture formation and deformation of lava crusts can be made by considering situations in which crust formation takes place largely after lava emplacement so that stresses related to lateral flow need not be considered.

Here we present both a detailed description of a fracture network cutting the surface crust of ponded pahoehoe basic lava from Tenerife and an analysis of the causative mechanisms. We document three scales of fracture development: a large set (metre-scale) of slabs bounded by orthogonal fracture sets, an intermediate scale (10–50 cm) more irregular rectangular to polygonal joint system and a small scale (1–10 cm) polygonal joint system. We show that the flow had largely come to rest before the crust started to become rigid so that the fracture system and surface topography are attributed to the effects of cooling, minor inflation of the lava, residual motions in the lava pond, and accumulation of gas bubbles below the crust. We develop a theoretical model

* Corresponding author. Tel. +44-(0)117-928-7789; fax: +44-(0)117-925-3385.

E-mail address: steve.sparks@bristol.ac.uk (R.S.J. Sparks).

[1] Deceased.

0191-8141/01/$ - see front matter
PII: S0191-8141(00)00089-4

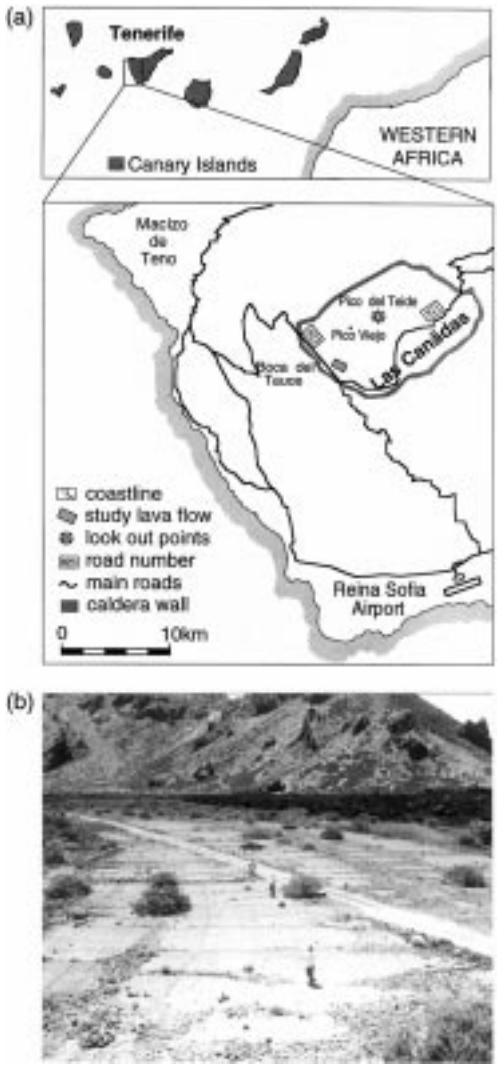

Fig. 1. (a) Location of the sampled lava flow within the Lavas Negras region of Las Canãdas, Tenerife. (b) View of the studied lava flow surface. Note the large-scale orthogonal fractures. The photograph is taken looking SSE parallel to the flow direction.

for the initial stages of cooling of a lava surface when radiation is dominant. This model is used to interpret field data and to help understand the role of tensile stresses related to cooling and crustal deformation. Field geometries and model results are used to support an interpretation that lava crusts are very weak, which has implications for understanding the role of cooling crust during lava emplacement.

2. Flow setting and characteristics

2.1. Geological setting

The volcanic island of Tenerife is dominated by a central caldera, Las Canãdas, at the centre of which lies the Pico del Teide at 3718 m and the Pico Viejo at 2994 m (Fig. 1a). This paper focuses on an exposure of the distal part of a single lava flow, which lies among several historic eruption products on the distal south-eastern flanks of the Pico Viejo stratocone (Ablay et al., 1998). The exposure lies immediately north of Boca del Tauce on road 823 (Fig. 1a). The lava exposure is close to the caldera wall in an area of generally very low slopes. It is a small area of a young basanite pahoehoe flow that erupted prior to a 1798 lava flow, which partially buries the northern margin of the exposure. Lavas from Pico Veijo are mostly aa flows, but small areas of pahoehoe are found at their margins. The pahoehoe areas typically emerge from aa flow fronts and local tumuli connected with tube systems.

2.2. Large-scale flow characteristics

The study area consists of a relatively smooth, flat lava surface over an area of approximately 3500 m^2 (Fig. 1b). The lava is less than a metre thick at its margins and slopes gently to the SSE in the direction of flow with an average slope angle of 0.6°. Perpendicular to the flow direction the average slope is negligible (<0.1°). The lava resembles the pahoehoe sheet flows observed on Kilauea volcano, Hawaii, which form on slopes of less than 1° (Hon et al., 1994). The surface is broken into a set of rectangular crustal slabs, 3–12 m wide and 3–11 m long, bounded by orthogonal fractures (Fig. 1b and Fig. 2), and typically 10–12 cm thick at the slab edges (Fig. 3). The crustal slabs are domed into low amplitude hummocks with typical heights relative to the edges of 5–20 cm. The hummocky topography causes local slope variations of as much as 6.2°, from a 2.9° slope towards the flow source to 3.3° in the inferred flow direction with comparable slope variations perpendicular to the flow direction. All margins of the lava sheet are buried by younger lavas except two. To the south-west, the lava margin is disrupted with crustal slabs tilted away from the margin, in a similar manner to the monoclinal margins of sheet flows on Hawaii, as described by Walker (1991) and Hon et al. (1994). Such morphology is related to the lava inflation by endogenous growth and uplift. A chaotic region of slab disruption occurs along the north-west margin.

Some slab boundaries are marked by narrow zones of younger lava (Fig. 4a), which were exposed to the atmosphere when the slabs rifted apart. The zones are typically a few centimetres wide, although they can be up to 50 cm wide. The thicknesses of the slabs were measured at these rifted ends. Slab thicknesses at the time of formation of the fractures were mostly in the 10–12 cm range (Fig. 3). The flow lineation on these fresh lava surfaces is oblique to slab margins, generally being oriented at 35–40° clockwise of the dominant NNW–SSE lineation on slabs. In one example (Fig. 4a), the zone is deformed by a low amplitude fold, with an axial plane parallel to the slab margins. The folded stretching-lineation indicates that oblique separation of the once adjacent slabs occurred prior to the localised shortening, normal to slab margins. In one area the stretching lineation and the fold are offset normal to the trend of the

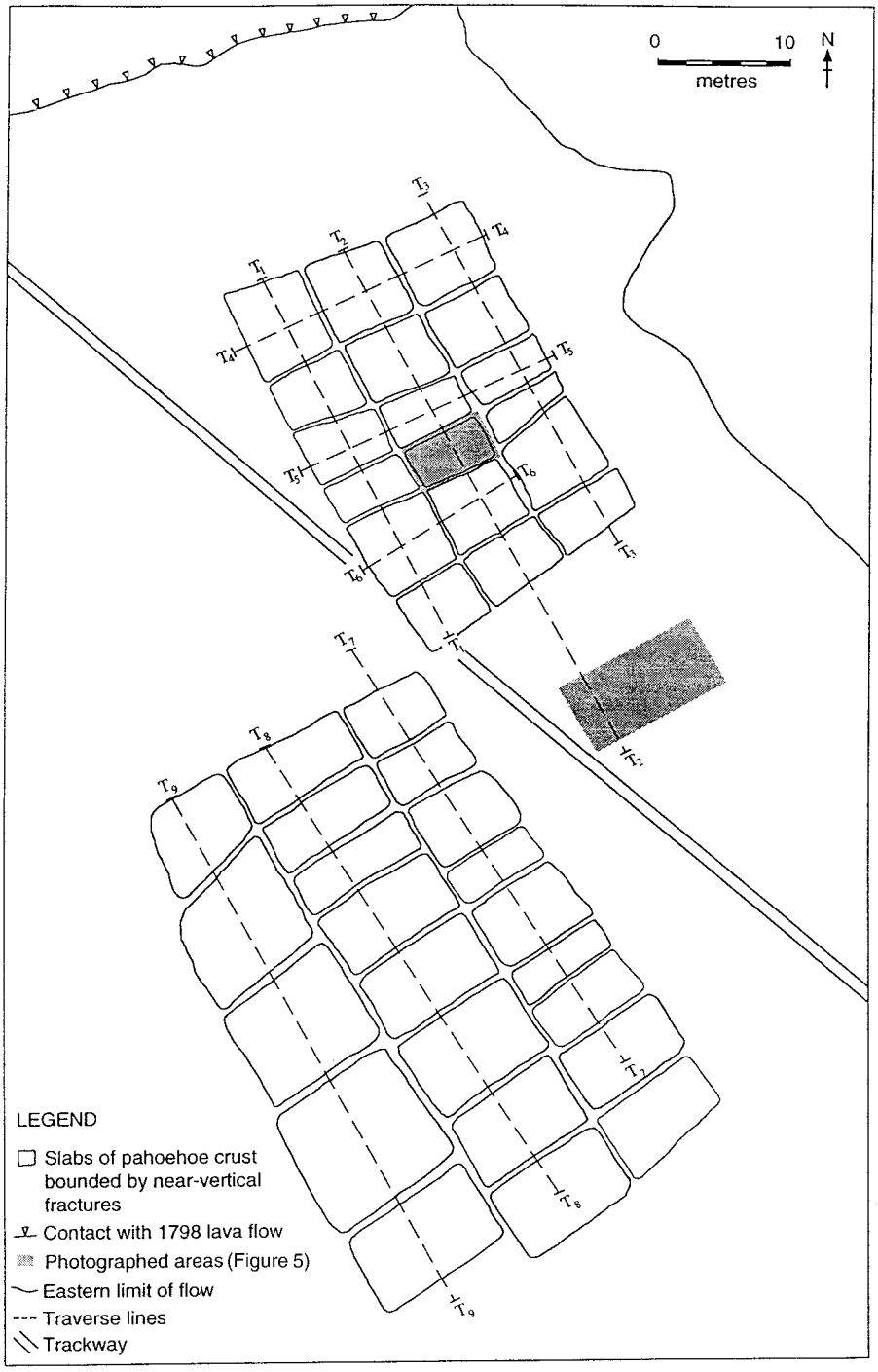

Fig. 2. Plan view of part of the lava flow, showing the large-scale rectangular blocks. The shaded areas were photographed to analyse small-scale joint networks (see Fig. 5). The location of scanlines, T1–T9, are shown.

fresh lava zone. These observations suggest that additional minor movements of lava occurred in its interior after the crust had formed and had begun to separate into the large-scale slabs.

2.3. Petrology

The lava is almost aphyric with a partly crystalline groundmass. The flow is a plagioclase basanite (Table 1; Ablay et al., 1998) and is part of the Pico Viejo series (Ablay et al., 1998). The top 10 cm of the lava crust contains on average plagioclase (28%), clinopyroxene (10%), olivine (3%), glass (58%), titanomagnetite (1.0%) and minor apatite. Glass content tends to decrease with depth from over 65% near the surface to about 40% at the base of the lava crust at 10 cm depth. Vesicle content of the lava crust

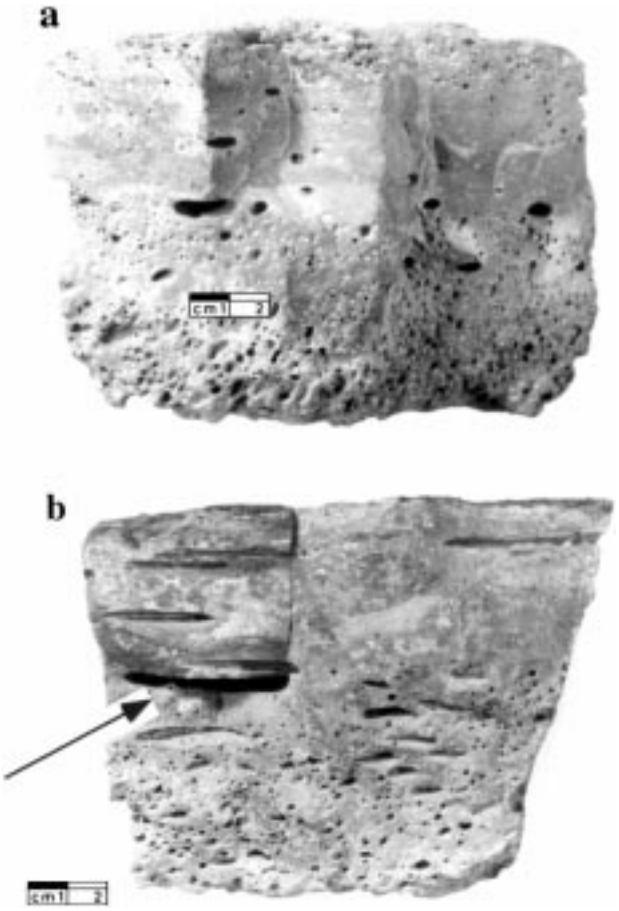

Fig. 3. Two samples of the flow crust. (a) Closely spaced joints in upper 4 to 5 cm merge with depth producing wider joints. (b) Joint-bounded block from the crust shows a vertical joint deflected by large elliptical vesicle (indicated by the arrow) to the left of prominent vertical crack in the sample. Note large deformed (more elliptical) vesicles in upper 5 cm.

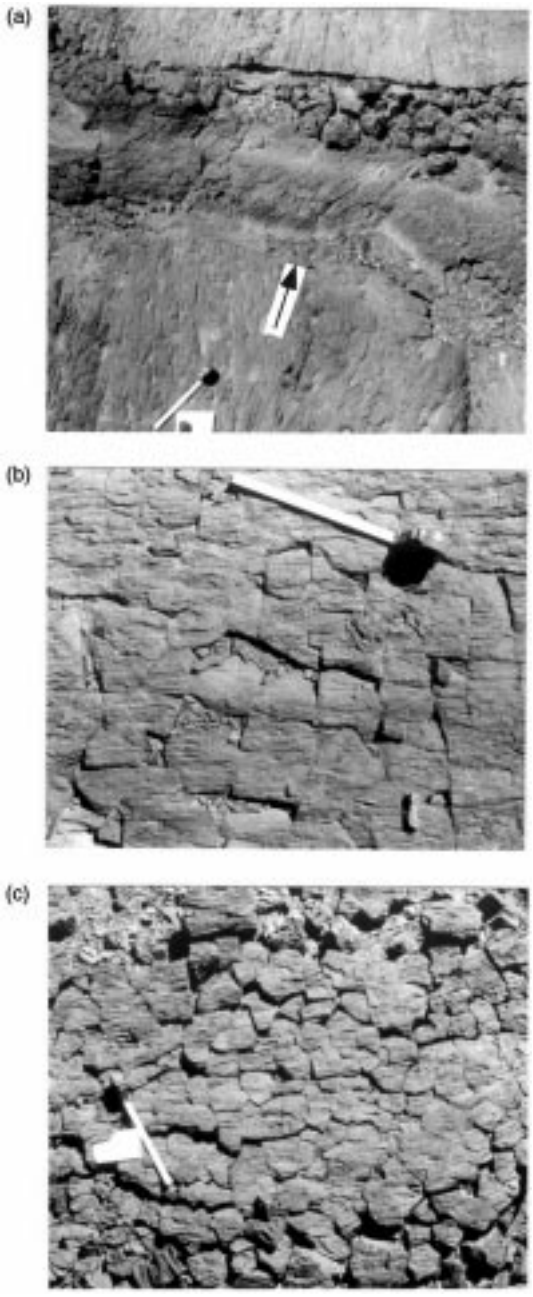

Fig. 4. (a) Zone between fracture-bounded crustal slabs that rifted apart obliquely, allowing a new lava surface to form in the gap. Arrow marks the slab edges. (b) Typical small-scale polygonal to rectilinear joints, many of which are parallel and perpendicular to the surface flow lineation. (c) Array of polygonal to rectilinear joints breaks the crust into well-defined blocks. Tape length in all photographs 25 cm. The tail of the tape measure points to the north.

averages about 9%, but varies from place to place with a range of 3 to 15% (Fig. 3) with the uppermost 3–4 cm of crust tending to have lower vesicle contents than the deeper parts of the crust. However, underlying lava was more vesicular than the crust with values of 30 to 40%.

Mineral analyses were determined by electron microprobe. Feldspar crystals range continuously from groundmass microlites to larger microphenocrysts and rare phenocrysts (<1%) up to 1.6 mm in length. Most crystals are between 0.05 and 0.30 mm in length and are not aligned. The average plagioclase composition is An_{56} varying from An_{49}–An_{76}. Many microlites are skeletal, which is typical of rapidly cooled lava. Pyroxene compositions fall into two distinct Ca-rich (Wo_{23-26}, En_{36-38}, Fs_{38-39}) and Ca-poor groups (Wo_{34-39}, En_{30-33}, Fs_{31-33}). The high calcic pyroxenes average 4.0% TiO_2, and low calcic pyroxenes average 2.6% TiO_2. Olivine compositions fall in the range Fo_{66}–Fo_{72}. A temperature of 1050°C has been calculated for the equilibrium between olivine and melt using the composition of olivine cores and the bulk lava composition (Röedder and Emslie, 1970). This temperature is similar to estimates made on other plagioclase basanites on Tenerife (Ablay et al., 1998). A residual glass (Table 1) has a tephri–phonolite composition. Estimates of temperature on other tephri–phonolite lavas on Tenerife indicate that the melt was preserved at about 950°C (Ablay et al., 1998).

Table 1
XRF analyses of two samples of plagioclase basanite lava (A and B) and electron microprobe composition of interstitial glass in the crust (C); nd means element not detected

Sample	A	B	C
SiO_2	47.31	46.72	57.35
TiO_2	2.94	2.84	2.29
$A1_2O_3$	18.29	18.39	20.44
Fe_2O_3	9.86	9.8	5.82[a]
MnO	0.15	0.15	0.22
MgO	3.18	3.45	0.74
CaO	8.06	8.26	1.24
Na_2O	6.32	6.95	5.31
K_2O	2.48	2.47	6.20
P_2O_5	1.05	1.05	nd
LOI	0.14	− 0.16	nd

[a] FeO for probe data.

2.4. Viscosity

Later we discuss lava emplacement and consolidation, and so viscosity estimates are needed. Melts with the bulk composition of the lava at the inferred eruption temperature of 1050°C have viscosities around 8×10^2 Pa s (Murase and McBirney, 1973; Ryan and Belvins, 1987), approximately $30\times$ greater than Hawaiian tholeiite at 1200°C. However, the lava was emplaced with suspended microlites and some microphenocrysts, so the emplacement temperature could have been below 1050°C and the effective viscosity could have been significantly higher. The residual tephri–phonolite glass preserved in the crust (composition C in Table 1) has an estimated viscosity of about 3×10^4 Pa s at 1050°C and 3×10^5 Pa s at 950°C, based on lava of similar composition investigated in Ryan and Belvins (1987).

3. Large-scale fracture network and hummocks

The upper surface of the lava flow is dominated by a well-developed, pervasive fracture network. Suborthogonal dominant fractures divide the flow into rectangular slabs of crust (Fig. 1b and Fig. 2) with the shortest sides parallel to a NNW–SSE flow lineation. T intersections indicate that the flow-parallel fractures developed before many of the flow-perpendicular fractures (Fig. 2). The slabs are slightly domed, sloping away from a peak near each slab centre, thus giving rise to a hummocky flow surface. Individual rectangular slabs are broken internally by a network of smaller-scale joints. In detail the slab-bounding fractures were influenced by these small-scale joints (Fig. 4a). This observation suggests that either the small-scale joints formed first or the tensile stress system that governed the small-scale network resulted in local perturbations of the larger scale stress system, causing local deviations in the orientation of the main slab-bounding fractures. Some of the slab-bounding fractures have minor fault activation, but most commonly have mirrored failure planes that gape open (Fig. 4a). For this reason we call these surfaces 'fractures', since this term encompasses joints, faults and cracks. Smaller-scale surfaces within individual crustal slabs are joints because they lack slip indicators. Although this small-scale joint network is irregular, a predominance of joints are preferentially oriented sub-parallel to the slab-bounding fractures (Fig. 5).

Traverses were made along six lines, each crossing at least three individual slabs, to measure the length, width and height of crustal slabs and the curved geometry of slab profiles (see scanlines on Fig. 2). An additional three traverses were made to collect width and length data on the western side of the trackway (Fig. 2). Measurements were taken by holding a tape horizontally so that it touched the highest point of a slab, and then the slab width and profile shape were measured. We recorded depths from the horizontal to the slab surface at intervals of 50 cm along transects perpendicular and parallel to the flow direction. Most slabs possess plan-form aspect ratios between 1:1 and 1:2 (Fig. 6). Most slabs show a single crest, but six have two crests. Slab height is defined as the vertical distance from the crest to a datum line between the slab ends in the direction of the profile. Height is harder to define for slabs with two crests. Heights were measured for the highest of the two crests relative to the datum line. The mean crest height was 9.5 ± 2.4 cm, a maximum of 19.6 cm and minimum of 4 cm. Slab length and height are well correlated for slabs with one crest (Fig. 7). However, slabs with two crests have the longest slab dimensions about twice that for single-crested slabs. Thus, the double-crested slabs are considered as two hummocks, which were not separated by fractures.

To compare profiles of differing lengths the data were normalised for maximum slab height and length to a range from 0 to 1.0 (Fig. 8). The influence of the flow slope was considered, as the attitude of the upper surface meant that many of the profiles had one fracture-bounded margin higher than the opposite one. To correct for this elevation, each profile was restored to an arbitrary horizontal datum. For those profiles with one crest, the change of height, h, with distance, x, from the crest to the end of a slab can be described approximately by a power law of the form $h\ \alpha - x^n$, where the exponent n mostly varies between 2 and 3. Data for the longest measured line from the crest to the end plot as a straight line on a plot of h versus the cube of the distance (Fig. 9a). Data on the maximum deflection of the slab edge against length from the slab crest to the edge are compared with linear, square and cube laws in Fig. 9b.

4. Small-scale structures

4.1. Flow surface lineation

The direction of flow emplacement is indicated by a surface lineation created by the alignment of vesicles at,

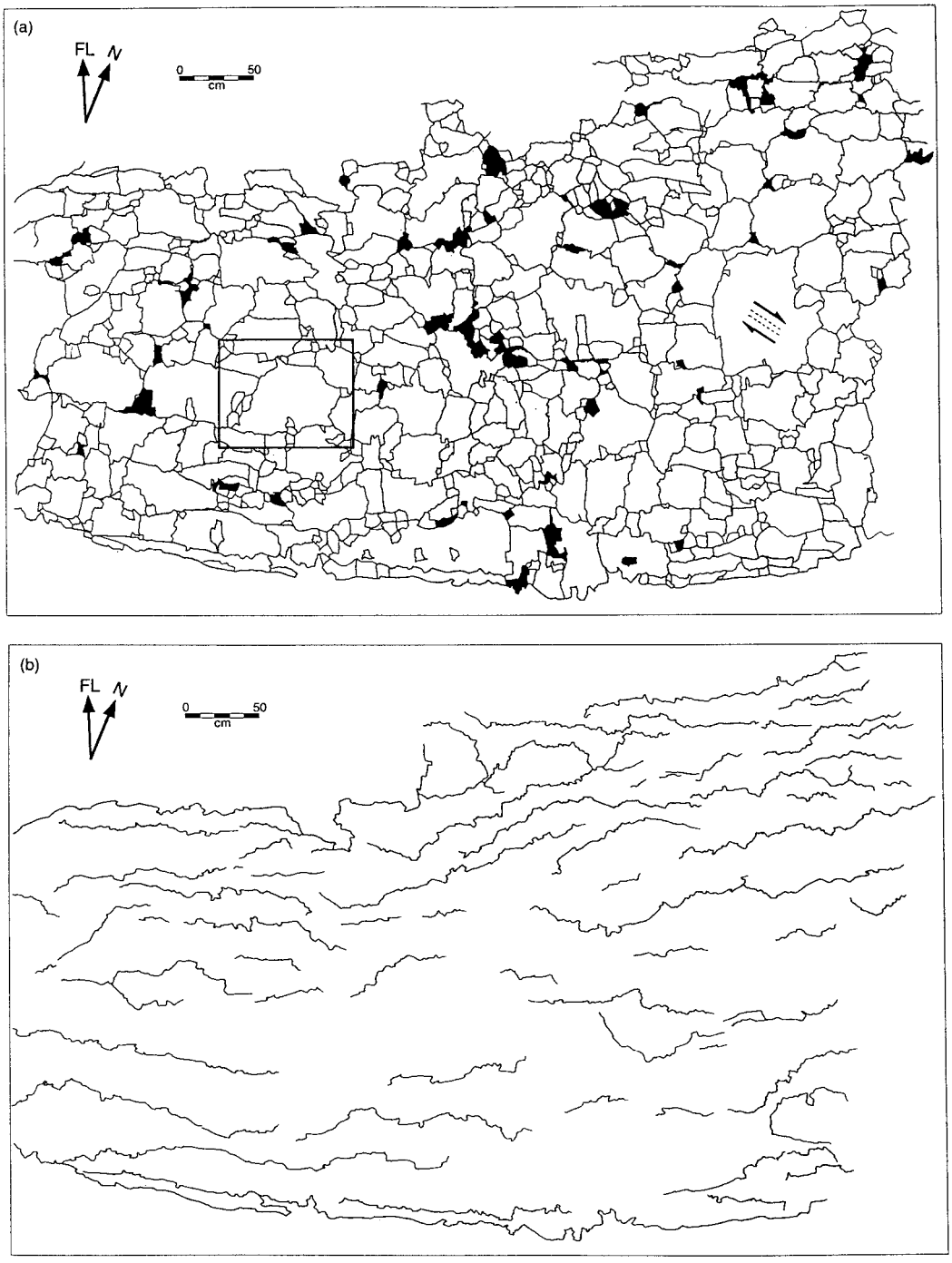

Fig. 5. (a) Joint network traced from the photomosaic of the more northerly shaded area marked of Fig. 2. Black areas excluded from analysis because their blocks are out of place. The largest block contains a minor shear zone with shear direction indicated by the arrows. (b) Pattern of emplacement-related, early-formed joints deciphered from the joint network in Fig. 5a. FL indicates the flow lineation direction which is parallel to one of the main slab-bounding fractures with the other slab-bounding fracture being perpendicular to the flow direction.

and near, the flow surface (Figs. 3 and 4). Formerly spherical bubbles were stretched into cigar-shaped vesicles, and indicate that stretching was parallel to the direction of former flow. Some bubbles ruptured at the flow surface to form an elongate depression. The flow lineation that dominates across the study area is oriented NNW–SSE. Near flow margins the lineation azimuth varies by as much as ± 50, suggesting lateral spreading of the lava away from the main flow direction. However, we interpret the fact that most of the area displays a systematic lineation means that the lava sheet was guided by a topographic depression oriented in the flow direction.

Stretched bubbles average 5 cm in length and are a few millimetres wide (Fig. 3). Where the surface has been

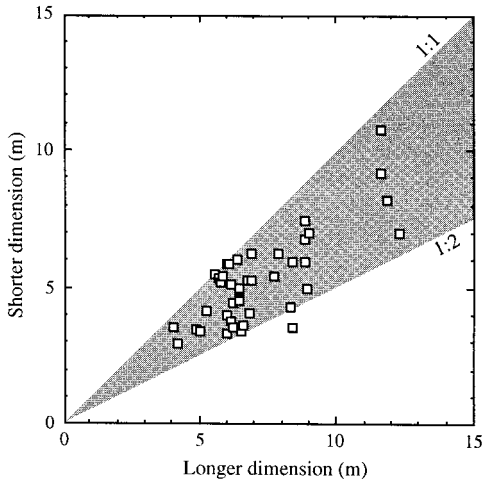

Fig. 6. Slab dimensions plotted as longer versus shorter dimension; 98% of data lie between aspect ratio lines 1:1 and 1:2.

extensively stretched the bubbles may be up to several decimetres in length. Most slabs of crust show that only bubbles within 2 to 5 cm of its upper surface are strongly deformed, whereas deeper vesicles are nearly spherical (Fig. 3). Some crust is banded with vesicle-rich and vesicle-poor zones (Fig. 3). The near-surface, highly elliptical vesicles suggest that the lava chilled rapidly on contact with the atmosphere, locking the sheared gas bubbles in place. Below 2 to 5 cm, the lava remained molten long enough for near spherical bubbles of several millimetres in diameter to be preserved (Fig. 3). Our data contrast with observations on Hawaiian tholeiite pahoehoe sheet lavas (Hon et al. 1994), where highly deformed vesicles are only preserved in the outermost 1 to 5 mm of the crust. Below we show that this difference can be attributed to the much higher viscosity of the Tenerife lava.

Shearing and elongation of the bubbles at the flow surface requires the surface to have been a region of strong shear

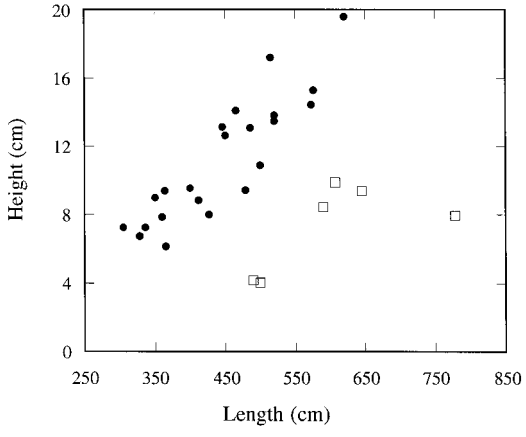

Fig. 7. Slab length or width plotted against height. Solid dots for slabs with single crest and open squares for slabs with two crests. Those with a single crest display a positive correlation, which can be fitted by a linear regression with a correlation coefficient of 0.89.

deformation. This cannot happen at a free surface. The observation that the most strongly deformed vesicles are at the surface, implicitly prior to development of a crust, also rules out shear between a crust and the underlying lava. In other lavas, such as those on Mt. Etna (Pinkerton and Sparks, 1976) and those on Hawaii (Hon et al., 1994) surface lineations form where lava emerges from lava tubes at secondary vents. The new flow surface emerges and detaches from the roof of the tube, which is a region of strong shear. This distal pahoehoe sheet is thought to have been tube fed, with the lineation developed as the ductile, vesicular lava emerged from the tube. A local variation of an otherwise uniformly oriented flow lineation is a 'swirl' or lava coil within the local lineation (Fig. 10). This phenomenon can be attributed to the action of a shear couple between two areas of developing crust moving at different velocities while the lava surface was still sufficently hot to be ductile. Differential motion develops shear instabilities deforming the pre-existing lineation into swirl-like folds.

4.2. Joint characteristics within crustal slabs

Representative areas of the flow surface were photographed to investigate the joint system within the large-scale crustal slabs. For larger areas, individual prints were pieced together into a mosaic to produce a detailed map of the fracture network in a typical slab interior (Fig. 5). The mosaics show that the slabs are internally segregated into blocks bounded by sub-orthogonal joints. The joint-bound blocks range from polygonal to crudely rectilinear in overall planform, but many block edges are irregular on a millimetre- to a-few-centimetre scale (Fig. 5a). Flow-normal joint traces tend to be straighter than flow-parallel joint traces. Blocks close to the margin of the flow are less equant in planform than those near the flow centre (Fig. 5a). There are two scales of blocks, as will be confirmed by a statistical analysis below. The larger blocks are bounded by significantly smaller blocks (Fig. 5a), particularly at the large block margins (Fig. 11) and where a joint bounding a larger block changes strike.

Areas near the margins of the large-scale crustal slabs are dominated by the small-scale joint networks (Fig. 4b and c). These areas have much more equant blocks bounded mostly by straight-sided and occasionally curving joints (Figs. 3 and 4). The blocks are rectilinear to polygonal and can be easily extracted to produce equant blocks of crust (Fig. 3). In profile, even smaller joints of 1 cm size occur close to the crust surface (Fig. 3a). The smaller joints disappear or merge into the larger-scale joints, which penetrate the complete slab thickness. Large vesicles deflect the fractures and even cause bifurcation (Fig. 3b). Also, the irregular jagged boundaries of intermediate-scale joints are controlled by the small-scale joints (Fig. 5).

The distributions of joint-bound blocks in terms of area were determined using image analysis software (Fig. 5a and Fig. 12). Two distinct block sizes are identified from the

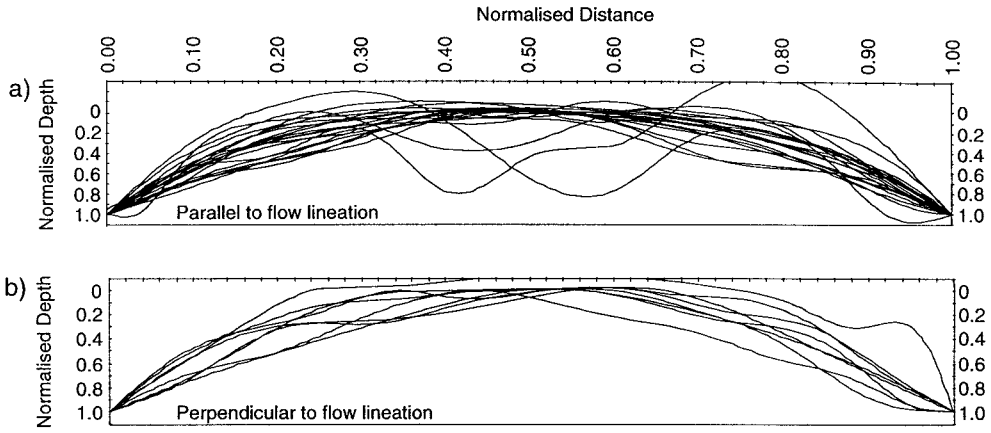

Fig. 8. Normalised slab profiles. (a) Slab data from scanlines T1 to T3 (parallel to flow lineation); some profiles show two peaks. (b) Slab data from scanlines T4 to T6 (profiles taken perpendicular to flow lineation).

presence of two peaks in an abundance of areas plot (Fig. 12a). Block areas can be separated into two log-normal distributions (Fig. 12b). In the particular slab area investigated (Fig. 5a), the large blocks make up 92% of the area and have a median value of 585 cm^2 with a 2σ range from 105 to 2350 cm^2. These areas correspond to a characteristic median width of 24.2 cm with a range of 10.5 to 48 cm. The small blocks make up 8% of the investigated area and have a median area of 34.8 cm^2, with 2σ ranging from 6.6 to 120 cm^2. These areas correspond to a characteristic median width of 5.9 cm with a range of 2.6 to 11 cm. An independent analysis of 59 small-scale blocks in the another area (Fig. 4b) is similar. The median area of blocks is 42.2 cm^2 with 2σ range from 14 to 105 cm^2, equivalent to a characteristic median width of 6.4 cm with a range from 3.7 to 10.5 cm. The characteristic block widths are approximated as the square root of the areas. Joint spacing was analysed by using scanlines parallel to the flow direction and spaced at 10 cm intervals (Fig. 13). Spacing increases into the slab with the range steadily increasing up to 50 cm from each margin.

Joint intersection analysis determines the relative age of abutting fractures. Most abutments are T-types, where younger joints terminate at older ones (Hancock, 1985). Studying all intersections determines the order of fracture linkage, and identifies if one set is uniformly younger than

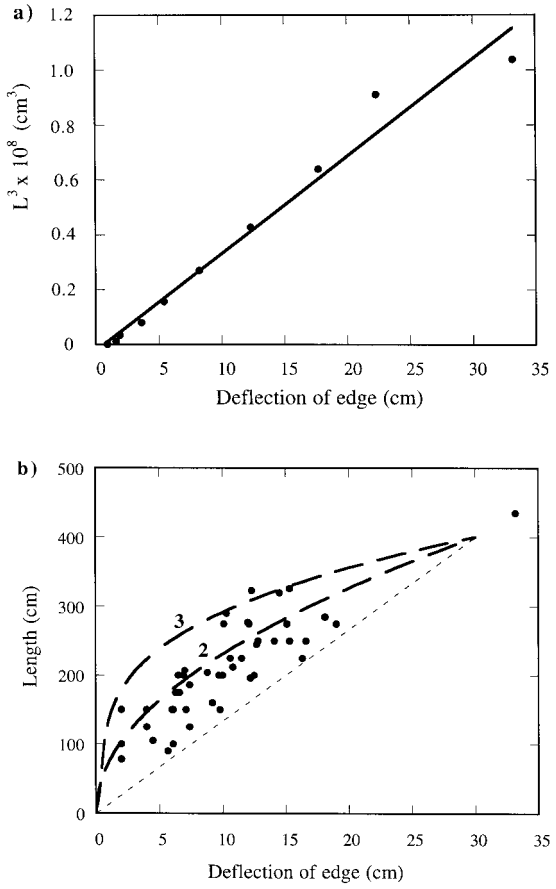

Fig. 9. (a) Example of height deflection of a slab relative to the crest plotted against the cube of the distance, L, from the crest. The best fit regression line is shown. (b) Deflection at the edge of slabs versus length from edge to crest. Two curves represent power laws with exponents 3 and 2 fitted through a point with $L = 4$ m and $h = 30$ cm. The dashed line is the linear fit through the same point.

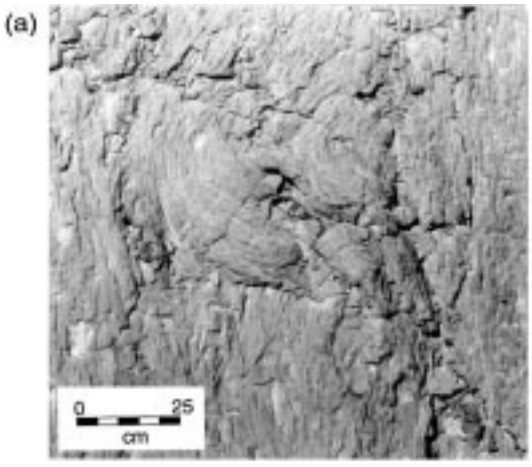

Fig. 10. A swirl appears as a near-circular perturbation within an otherwise uniform flow lineation.

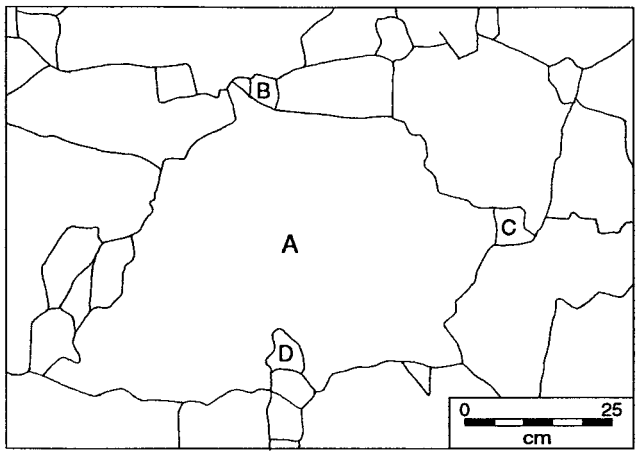

Fig. 11. Enlargement of part of Fig. 5a showing smaller block fragments within larger blocks of crust. Block A has smaller fragments, B, C and D, which share common joint segments with it.

another. 1500 intersections were assigned to one of four groups depending on the orientation of the T-junction with respect to the flow direction (Fig. 5a and Fig. 14). More NNW–SSE (flow parallel) joints abut ENE–WSW (flow perpendicular) joints than vice versa by a ratio of 2.3:1. Thus, we conclude that many flow-perpendicular joints developed before flow-parallel joints. Close analysis of the junctions of the early formed, flow-perpendicular joints showed that many are arranged adjacent to each other and link to make a large-scale, early-formed (primary) joint system (Fig. 5b).

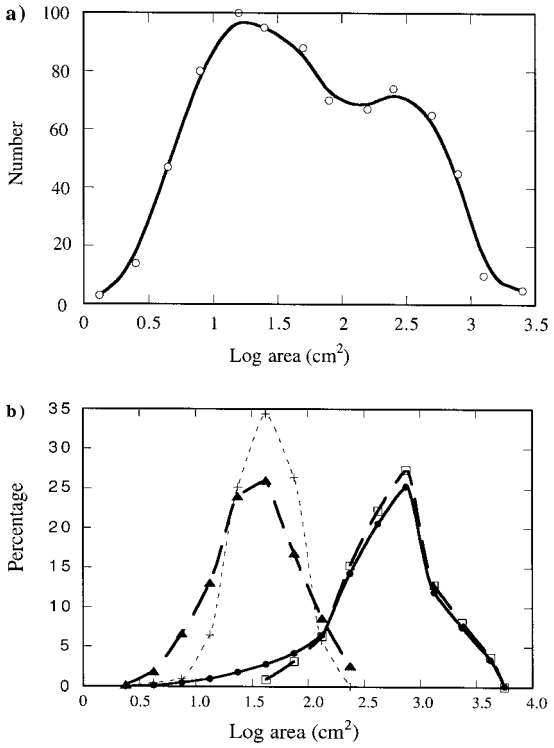

Fig. 12. Joint network characteristics for Fig. 5a. (a) Number of fracture-bound blocks in terms of log of the area of individual fracture bound blocks. Peaks occur at 16 cm^2 and at 252 cm^2. (b) Percentage of total area by block size (bin interval in 0.25 log units) for all blocks in Fig. 5a (solid circles), large blocks in Fig. 5a (open squares), small blocks in Fig. 5a (crosses) and all blocks in Fig. 4b. Two sub-populations are differentiated by segregation into two log normal distributions.

5. Surface cooling of ponded lava

A model is developed to describe the early solidification of a molten, sub-aerial lava sheet that incorporates features observed in the Tenerife lava. The aim is to predict the free-surface crust growth rates, the surface temperature and the thermal structure in the solidifying crust to help constrain interpretation of the features. Fig. 15 illustrates the growth of a free surface crust in the lava and the parameters that control its advance into the flow interior. We focus attention on the upper surface of the sheet, where heat is extracted into the overlying atmosphere, and consider the early heat loss behaviour.

The lava sheet is assumed to consist of a stagnant homogeneous liquid with constant thermal properties in both phases, liquid and solid. It is emplaced with negligible superheat at a maximum temperature of 1050°C, as suggested by minor large phenocrysts (<1%). The lateral dimensions of the sheet are large in comparison to the depth of solidified crust and so the problem is essentially one-dimensional. Thermal convection within the lava interior is ignored because the time scales required for thermal convection to become important are much longer than the time frame in the model (Worster et al., 1990). Crystallization within the melt is treated as releasing latent heat per unit volume, L. Heat loss from the upper surface is modelled by a combination of radiation and turbulent natural convection in the overlying air. The model is also modified to take account of the effect of vesicles on the thermal conductivity of the crust.

A comparison of these two modes of heat transfer shows that over the desired time scale of the model, which is approximately 8 h, both modes are of comparable importance with radiation dominating at early times and natural convection at later times. The detailed development of the model and the numerical method are given in Appendix A. The model is similar in broad terms to previously published models of crust growth (e.g. Hon et al., 1994), and has been developed here for specific application to the situation on the Tenerife lava.

Calculations use the following estimated thermal property values for the plagioclase basanite lava: specific heat 0.38 cal gm^{-1} K^{-1}, thermal conductivity 0.005 cal gm^{-1} cm^{-1} K^{-1}, heat of crystallization 100 cal gm^{-1} (Provost and Bottinga, 1972; Worster et al., 1990) and an assumption of 50% crystallization. We take the base of the crust to be the 950°C isotherm and the interior temperature to be 1050°C. The crust base isotherm is somewhat arbitrary, but the choice of 950°C will be justified approximately

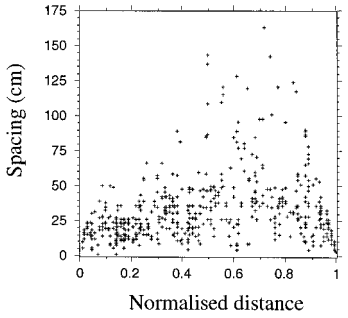

Fig. 13. Graph showing the spacing of emplacement-related joints, measured perpendicular to flow direction, across the width of individual crustal slabs.

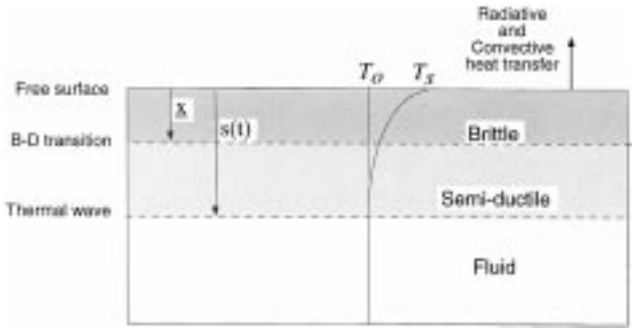

Fig. 15. Cross-section through an idealised lava flow, showing growth of a free surface crust. Here x is the distance from the crust surface and $s(t)$ is the position of an isotherm which defines the boundary between the crust and fluid interior.

a posteriori. Radiation is the dominant mode of heat transfer during the formation of the slabs (Fig. 16). Surface temperature declines to below 700°C in the first few minutes (Fig. 17a), and a more gradual decline in surface temperature to about 300°C over the first 8 h (Fig. 17b). The calculations indicate that the time scale for forming the 10- to 12-cm-thick slabs is 2–3 h (Fig. 18) and that the first 1 cm of the crust forms within 160 s. The results of these thermal calculations are consistent with cooling observations on the surfaces of pahoehoe sheet lavas in Hawaii (Hon et al., 1994).

6. Development of the fracture system

We now consider formation of hummocky topography, of crustal slabs bounded by a large-scale rectilinear fracture network, and of the intermediate and small-scale joint system. The analysis leads to the proposal that the crust becomes divided into three zones with different physical properties and responses to deformation. The analysis is used to infer that lava crusts are weak, which has implications for understanding the role of crusts in lava emplacement.

6.1. Initial emplacement

The Tenerife pahoehoe lava was emplaced to form a local area of ponded with a very gently sloping surface (0.6°) and lateral margins about 1 m thick. The vesicular flow emerged from a lava tube, producing a surface lineation. The uniform direction of the lineation indicates emplacement into a depression confined at its margins to form a lava pond. The ponded flow started to cool and formed a crust. Little deformation of the lineated surface can unequivocally be associated with initial emplacement. We thus infer from the well-organised rectilinear network of fracture-bound slabs that lateral motion of the lava had largely ceased before the process of crust formation started. The thermal modelling indicates that the surface temperature would have decreased to below 700°C after about 3 min of exposure of the surface to the air (Fig. 17a). Rheological stiffening of the very near surface, due to crystallization and cooling, should thus cause a rigid crust to start developing after a few minutes. Surmising that the lava was largely emplaced in a time shorter than the time for a rigid crust to develop, then the lava pond initially formed as a rapidly moving flood, perhaps related to a burst out from a nearby lava tube. The exposure is 80 m long so a speed of at least 0.3 m/s is implied.

There were, however, some residual motions, including

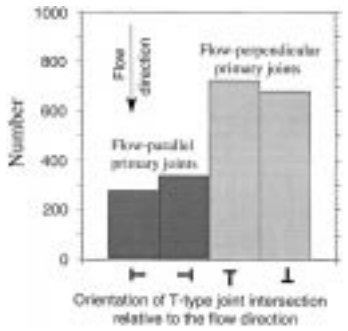

Fig. 14. Plot of the abundance of T-type junctions by orientation to the flow direction for Fig. 5a.

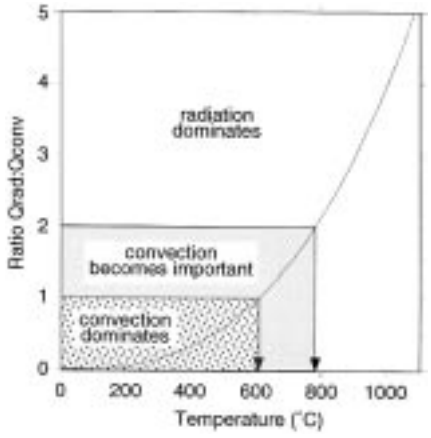

Fig. 16. Comparison of the relative surface heat fluxes for radiation and convection, during lava cooling in the first 4 h following eruption.

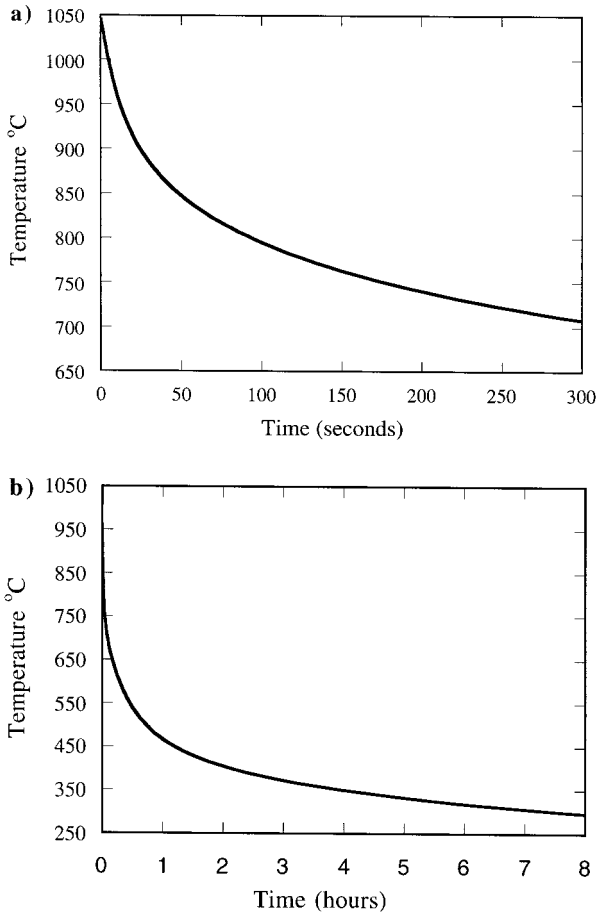

Fig. 17. Lava surface temperature calculated as a function of time over 300 s (a) and 8 h (b).

evidence of further slow supply, causing lava inflation features at the flow margin. Observations from Hawaii (Hon et al., 1994) indicate that inflation can occur quite passively with uplift of the surface crust. Thus, the lava pond may well have been fed internally by further influx while the crust was growing. Some local differential shear also occurred between some slabs in the earliest stages of crustal growth, with occurrence of swirl structures (Fig. 10).

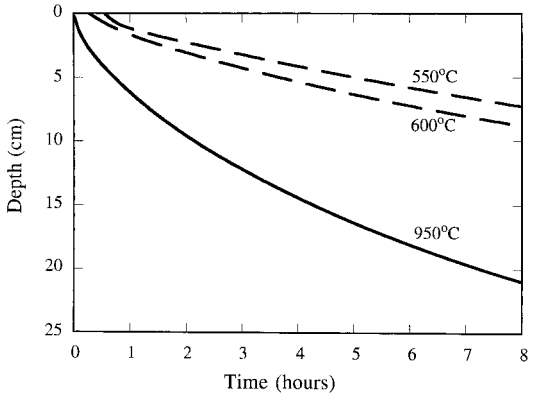

Fig. 18. The calculated positions of 950°C, 600°C and 550°C isotherms during surface cooling. The 950°C isotherm is taken as the base of the crust.

Otherwise, the surface quickly became stagnant. The interpretation that conditions were largely stagnant during crust growth is supported by the absence of any flow foliation defined by crystals, and the spherical shape of bubbles in all but the outermost 2–5 cm.

The cooling model can be used to interpret observations of deformed bubbles in the outermost crust (Fig. 3). The time scale, t, for bubbles radius, r, to return from a deformed state to a spherical shape is calculated from

$$t = \frac{\mu r}{\sigma} \quad (1)$$

where μ is the viscosity and σ is the surface tension. For a bubble radius of 5 mm, viscosity of Hawaiian basalt of 30 Pa s, and surface tension of 0.05 Nm^{-1}, the time is of order 5 s. The thermal model suggests that deformed bubbles would only be quenched into the outermost few millimetres of Hawaiian lavas, consistent with observations (Hon et al., 1994). For a typical bubble radius of 1 cm for the Tenerife lava (Fig. 3) and viscosity of 800 Pa s the time scale is 160 s. According to our cooling model the crust reaches about 1.0 cm thick at this time. The preservation of deformed vesicles in the uppermost 2–5 cm of crust implies that the viscosity was rather higher than our estimate of the melt viscosity at 1050°C. The time scale for forming crust in the 2–5 cm range is 1000–3000 s (Fig. 18). Applying Eq. (1) then the implied viscosities are 5000–15000 Pa s. The upper value is close to the estimated viscosity of the residual glass at 1050°C (see Section 2.4). Higher viscosity can be attributed variously to the effects of crystals and an evolved residual melt, to some cooling of the lava at the margins of the feeding lava tube prior to extrusion of the pahoehoe sheet, and the possibility that the lava was in fact emplaced at a somewhat lower temperature than the maximum of 1050°C.

6.2. Crust definition and properties

Before discussing the origin of the crustal deformation features and fracture networks we consider the definition and mechanical properties of the crust. At any stage in crust growth a continuous vertical temperature variation exists and therefore continuous variations in physical properties from a Newtonian lava in the hot interior to an elastic solid at the cold surface. Choosing a specific temperature for the boundary of the crust is to some extent arbitrary, although in Hawaiian tholeiitic lava lakes there are large physical properties when groundmass crystallization approaches the condition of close-packing at around 55% crystals and 1065°C (Peck, 1978), making this temperature a practical choice. Hawaiian lava below 1065°C is largely crystalline with little residual glass so it is a reasonable approximation to also regard this temperature as defining the brittle–ductile transition. In the much more evolved Tenerife lava we have chosen 950°C as the isotherm to mark the crust boundary. Samples from the base of the crust are about 60% crystalline, indicating that here too a

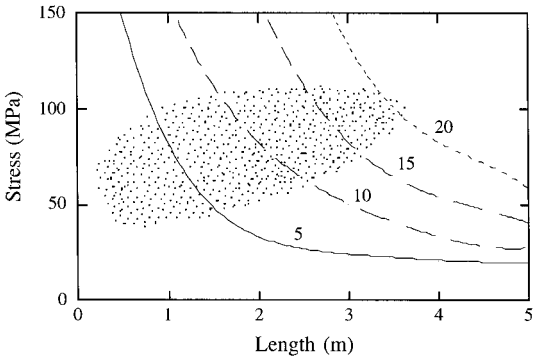

Fig. 19. The theoretical tensile stress from bending a horizontal plate into a curved segment due to a central force is plotted against the distance between the plate centre and edge. Curves are shown for values of uplift of 5, 10, 15 and 20 cm. The stippled area shows uplift heights and lengths observed in the Tenerife crustal slabs.

close-packing condition provides an approximate definition of the transition from crust to mobile interior. The concept of a brittle–ductile transition is not straightforward in material containing substantial amounts of glass or melt. The transition depends on strain rate, glass composition, and temperature (Dingwell and Webb, 1989; Dingwell, 1998). Thus, stress increase towards failure, and fracture formation can only occur when the time scales of deformation exceed relaxation times of the melt. Consequently for the Tenerife lava, the brittle–ductile transition cannot be known independently of the deformation history of the material.

6.3. Origin of large scale fracture network and hummocky slabs

Two observations help constrain the timing and origin of the large-scale hummocky crustal slabs. First, the crust was about 10–12 cm thick when the slabs rifted apart to form the rectilinear network of large-scale fractures. Our thermal model indicates that about 2–3 h is needed for this amount of crust growth (Fig. 18). Thus, whatever process is invoked to explain the fracturing requires a relatively slow build up of stress. Second, those slabs with two crests are interpreted to indicate that the surface deformation process started prior to the formation of the bounding fractures, and that slab doming was a cause of fracture development rather than a consequence.

Peck and Minakami (1968) observed comparable hummocks on crustal plates in the Hawaiian Makaopuhi lava lake and related them to the trapping of gases exsolved from the volatile lava beneath the solidified crust. The lava below the crustal slabs of the Tenerife lava is much more vesicular than the crust and so their model also seems plausible here. Typical bubble sizes observed in the Tenerife lava are several millimetres in diameter (Fig. 3) and are estimated to take only a few hours to rise in a stagnated lava pond. For example, using Stokes law, bubbles with diameters of 5 and 10 mm are estimated to take about 6 and 1.5 h respectively to rise through a metre thickness of lava with a viscosity of 800 Pa s. Thus, the time scale required to trap significant amounts of rising gas bubbles beneath the growing crust is consistent with development of deformation at a time when about 10 cm of crust had formed. The pocket of gas or vesicular lava provides a buoyant force, which uplifts the crust locally. Once the crust starts to rise then the uplift centre will form a focus for lateral gas flow and gas entrapment, accentuating the effect. We acknowledge that a weakness in this model is that it does not account for the spacing of the centres of uplift. We do not have a convincing explanation of what controls spacing, though one speculation is that the spacing is related to bubble-aided convection in the molten interior of the lava.

The major bounding fractures are parallel and normal to the flow direction. We therefore suggest that the fractures are also influenced by the geometry of the flow margins, which are also normal and parallel to the lineation. The geometry suggests extension along and across the flow. Walker (1991) and Hon et al. (1994) have documented endogenous growth of flat-lying pahoehoe lavas, which result in gradual thickening after initial emplacement by further slow lava supply. Characteristically, the margins develop tilted blocks and clefts similar to those observed on the south-west margin of the Tenerife lava. The lava sheets inflate and then spread outwards deforming the flow edges. This process will cause extension normal to both the flow margins and the flow front in the interior of the sheet. We therefore suggest that endogenous growth influenced the orientation of the large-scale slab-bounding fracture system. In this model, extension should be slightly greater in the down-slope direction, as is observed, and is consistent with the short dimension of the slabs always being parallel to the flow lineation.

As the crust deforms into a hummock, lateral stresses will build up and we postulate that the fracturing develops when these stresses exceed the crustal tensile strength. Arching of the surface between two crests create tensile stresses because the distance along the surface between the two fixed points defined by the crests must increase during uplift. The tensile stress change caused by bending deformation can be calculated as a function of uplift and distance, $2L$, between two crests (Fig. 19) in the range of observed crest separations (3–10 m) and the range of observed uplifts (2–20 cm). The bent surface is approximated as part of a circle of radius $R = (L2 + h2)/2h$, where h is the crest height. The strain along the length of a horizontal line deformed into this curve with the two crests remaining as fixed ends is given by:

$$\varepsilon = \pi\left[\left(L^2 + h^2\right)/h\right]\left\{\tan^{-1}\left[2hL/\left(L^2 - h^2\right)\right](1/180)\right\} - 2 \quad (2)$$

The tensile stress can then be estimated from Hookes

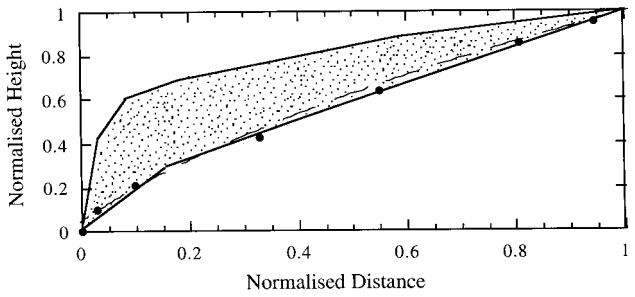

Fig. 20. Plot of normalised height versus normalised distance from the crest (top left) to the edge (bottom right). Dashed curve is theoretical profile from Eq. (6). The stippled area is that bound by range of shapes for crustal plates with a single well-defined crest (Fig. 8).

Law, Eq. (2) and observed uplift values. For a Youngs modulus of 2×10^{10} Pa (Murase and McBirney, 1973), uplifts of order 10 cm are easily sufficient for failure conditions to develop. Stresses of several megapascals to tens of megapascals fall in the range of many crystalline rocks with tensile strengths of a few megapascals and flawless volcanic glasses with strengths of order 100 MPa (Dingwell, 1998).

We now consider the shape of crustal slabs away from their crests after fracturing has occurred. The crustal slab is treated as a cylindrical elastic plate with a point force at the centre with the ends free. This is the simplest configuration where an analytical solution exists (Hearns, 1989). Different configurations such as a plate with distributed loading and a plate with clamped ends give results similar to the case of a point force and free end, differing only in detail. The profile of the circular plate is given by

$$h = 3F\left(1-\nu^2\right)x^2(3+\nu)(1-\nu) \times\{[\log_e x - 1] - 0.5[2\ \log_e L + 2.83]\}/2\pi E\delta^3 \quad (3)$$

where h is the deflection, F is the point force, ν is Poissons ratio (taken as 0.33), x is the radial distance from the plate centre, L is the plate radius, E is Youngs modulus, and δ is the slab thickness. The maximum deflection at the plate edge (equivalent to the crest height in our description of the slab heights) is related to the plate radius as follows

$$h_{\max} = 3FL^2(3+\nu)(1-\nu)/4\pi E\delta^3 \quad (4)$$

For the application to the lava slabs, there are two instructive end member cases. First the force is taken as the excess weight of the slab due to its density difference with the underlying vesicular lava, $\Delta\rho$, and thus the force will be proportional to slab size with Eq. (4) rewritten as

$$h_{\max} = 3\Delta\rho g L^4(3+\nu)(1-\nu)/4E\delta^2 \quad (5)$$

where g is gravity. Second, the force can be considered to be a constant irrespective of slab size. Such a situation might arise with the accumulation of a fixed volume of vesicular lava beneath the crust of each slab. Comparison of Eqs. (4) and (5) indicate that the maximum slab deflection should vary as a power between 2 (constant force in Eq. (4)) and 4 (force proportional to slab mass in Eq. (5)). These predictions are consistent with the observed trends (Fig. 9) with a power of 2 being the most consistent.

The profile of an individual slab can be compared with Eq. (3). The normalised profile of the slab obeys a slightly modified square law with the following form:

$$h/h_{\max} = (x/L)^2K\{[\log_e x - 1] - 0.5[2\ \log_e L + 2.83]\} \quad (6)$$

where K is a constant if the slab thickness and slab elastic properties are constant. This result is plotted in Fig. 20 and compared with the range of plate profiles from Fig. 8. The theoretical profile compares well with the less contorted slabs, but many slabs depart from this prediction with more pronounced bending, particularly towards the slab edge (Fig. 9a). Several possible explanations arise. The slabs are not circular plates but rectangles with additional mass at the corners. The free edges of the slabs are also denser than the underlying vesicular lava so they may have started to sink before being frozen in. Below in Section 7, we also propose a further explanation for the more pronounced deformation based on a conceptual model of the crust.

We now compare the predicted edge deflections with observations. We have chosen $L=$ 3 m, $\delta=$ 0.1 m, $E=2\times10^{10}$ Pa, and $\Delta\rho=500$ kg m^{-3} as typical values for the Tenerife slabs, and $g=9.81$ m s^{-2}. We calculate the maximum deflection as only 0.33 cm using Eq. (5). This result shows that the crustal slabs are much more deformed than expected for an elastic plate model. None of the physical property values can be changed to within plausible limits to values which could account for deflections of the order 10 cm. An alternative approach is to use the observed deflections to estimate the crust thickness required to produce the observed deflections. Taking $h_{\max}=0.1$ m and $L=3$ m then the plate thickness is calculated at 1.8 cm. In Section 7, we suggest that this result is physically meaningful.

An alternative explanation of the large-scale hummocks is that they result from differential contraction of the cooling crust (K. Hon, personal communiation). For this explanation the deeper crust contracts more than the near surface crust, so that a stress gradient develops and causes the slab to bend. However, cooling and thermal contraction is fastest at the surface so differential contraction would be expected to cause the plate to buckle with the edges moving up rather than down. While this process cannot be excluded, it has other problems. As discussed in more detail below, the small-scale joints, bounding polygonal blocks, are interpreted to result from thermal contraction. The stresses induced by thermal contraction had already developed in the crust prior to the formation of the slab-bounding fracture system. Furthermore small-scale thermal joints scale with the crust thickness, whereas the slab-bounding fractures do not. Thermal contraction cannot simultaneously produce

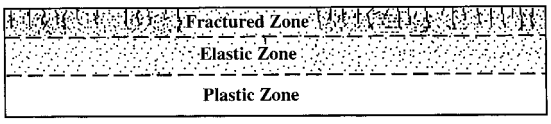

Fig. 21. Conceptual model of the lava crust divided into three zones.

fracture sets with very different scales and geometries. In addition we will argue in Section 7 that the hotter deeper parts of the crust behave plastically, because strain rates related to cooling are too slow to allow build up of tensile stresses.

6.4. Origin of intermediate and small scale joint networks

We have found two characteristic scales of joint-bound block within the large crustal slabs. The intermediate-scale blocks are of order 25 cm and are therefore 2–3 times wider than the crustal slabs are thick. The small-scale blocks are of order 6 cm and therefore have widths comparable to, but on average slightly less than, the crustal thickness.

The small-scale joints are interpreted as cooling joints caused by thermal contraction. In plan-view (Fig. 4) the joints have characteristic polygonal geometries with curving and planar boundaries as observed in other cooling joint systems developed on lava surfaces (e.g. Budkewitsch and Robin, 1994). The fractures also show the characteristic merging of initial small scale fractures near the surface (order 1 cm) into larger-scale fractures (several centimetres) at greater depth (Fig. 3). This increase is fracture size with depth reflects the approximate scaling of the joints with crustal thickness and the influence of cooling rate on the distance of fracture propagation. De Graff and Aydin (1993) have developed a thermo-mechanical model of joint propagation in lavas to explain the systematic increase in joint spacing with depth.

The intermediate-scale fractures, although in detail quite complex, are dominated by fractures either parallel or normal to the slab margins and therefore also parallel and normal to the surface flow lineation. We attribute these fractures to the bending of the crustal slab during hummock formation. As the slab bends, tensional stresses are expected to develop parallel to the margins of the slab, accounting for the rectilinear character of this joint network. Joint intersection data show that the joints perpendicular to the flow direction and parallel to the long axis of the slab analysed in detail developed earlier (Fig. 5a and Fig. 14). Additionally the gaps between slabs tend to be larger in the flow direction. We attribute the earlier development of the flow-perpendicular intermediate fractures to the addition of the down-slope gravitational component of the slab weight. Spacing of the intermediate joints is also closer at the slab edges, which we attribute to greater flexure near the edges.

7. The weakness of lava crust

Here we draw together the observations and discussions of the Tenerife lava to develop the idea that lava crusts are rather weak (Fig. 21). During its growth, the crust is strongly zoned in temperature, mechanical properties, and stress distribution. These variations are manifested in three postulated zones: a fractured zone where tensile stresses due to cooling and crustal deformation have been sufficient for jointing to develop; a middle elastic zone of elastic deformation and build up of body stresses due to cooling and crust deformation; and a plastic zone where no stresses can build up. These three zones need not exist at the same time and the boundaries between them depend on both temperature and strain rate as shown below.

The development of these conceptual zones can be considered in relation to recent advances in understanding the physical properties of silicate melts and glasses (Dingwell, 1998) and the nature of the brittle–ductile transition in silicate melts. The brittle–ductile transition is defined on the basis of comparing the time scale of deformation (the reciprocal of the strain rate) with the relaxation time of the silicate glass (Dingwell and Webb, 1989). When the strain rate time scale exceeds the relaxation time scale, defined as the ratio of viscosity to the shear modulus, stress builds up and is stored by elastic strain. The glass can fracture if the tensile stress exceeds its tensile strength. The brittle–ductile transition is approximated as points where these two time scales are equal. Thus, the boundaries between the three zones in Fig. 18 are not just functions of temperature, but relate to local strain rate, and the practice of using an isotherm to define crust thickness is a potentially misleading simplification.

These principles can be illustrated in the context of the Tenerife lava crust as follows. We estimated a characteristic strain rate during crustal doming by noting that it takes about 2 hours to grow a 0.1 m thick crust (Fig. 18). The estimated tensile stresses are typically of order 10 MPa (Fig. 19), giving a strain of 10^{-3} and strain rate time scale of order 10^{7} s. Strain rates due to cooling can be estimated by noting that the surface of the lava cools by 600°C in about 1 h (Fig. 17b), corresponding to a line length change of about 10^{-2} for a thermal expansion coefficient of 2×10^{-5} K^{-1}. This yields a strain rate of about 3×10^{-6} s^{-1} strain rate and a time scale of 3×10^{5} s. If the locus of the brittle–ductile transition of the glass is known, then the temperature against relaxation time scale diagram of Dingwell and Webb (1989) can be used to estimate temperatures below which elastic deformation and brittle behaviour can be expected for these strain rates. Unfortunately there are few data at low temperatures for glasses and none for the exact tephri–phonolite composition of the Tenerife lava. As an approximation, we assume that the glass behaves like the andesite melt investigated by Neuville et al. (1993), which has similar content of network forming $SiO_2 + Al_2O_3$ to the tephri–phonolite glass. The brittle–ductile transition

temperature is estimated to be 600°C for deformation related to cooling and 550°C for deformation related to crustal bending. These isotherms are plotted on Fig. 18. The crust above the isotherm at any given time is expected to respond elastically with stress build up, while the higher temperature crust below this isotherm is expected to deform plastically.

Consider now the situation when the 950°C isotherm reaches a depth of 10 cm after 2 h of cooling. We have two independent methods for estimating the elastic zone thickness. Theory for the bending of an elastic plate (Section 6.3) estimated an elastic zone thickness of 1.8 cm. The estimate of elastic zone thickness from the cooling model is also about 2 cm from the position of the 600°C isotherm. The two methods give similar results. Thus, we can explain the much more pronounced bending of the crust by invoking a thin upper elastic zone defined by a glass transition at 600°C.

At another extreme, consideration can be given to strain rate conditions when the large slabs rifted apart along large fractures penetrating to 10 cm depth. We surmise that these fractures initiated in the brittle zone, and were influenced by the build up of cooling stresses and small near surface joints. Fractures typically propagate at speeds of order 1 km/s (Anderson and Grew, 1977) and so the time scales for deformation are of order 10^{-4} s^{-1}. Using the temperature against relaxation time diagram of Dingwell and Webb (1989), we estimate the brittle–ductile transition to be at about 950°C. Thus fractures can penetrate through the 'low strain rate' brittle zone and penetrate deep into the plastic zone, justifying the choice of the 950°C isotherm as the base of the crust *a posteriori* on the basis that it is the depth to which fractures can penetrate.

We consider the time of formation of the small-scale thermal joints that are expected to initiate the formation of the fractured zone (Fig. 21). Using 600°C as the temperature below which thermal stresses can build up, our cooling model gives a time of about 1000 s for the surface temperature to fall below this temperature. Thereafter we expect that an elastic crust would grow with cooling-related tensile stresses increasing. A vertical gradient of tensile stress would be anticipated from zero at the 600°C isotherm to a maximum at the crust surface. We can use an approach by Peck and Minakami (1968) in their analysis of columnar joint development. The tensile strength, σ_T, can be related to the temperature difference, ΔT, by

$$\sigma_T = E\alpha\Delta T/(1-\nu) \quad (7)$$

where α is the linear coefficient of thermal expansion. Here we take $E = 2\times10^{10}$ Pa, $\nu = 0.33$ and $\alpha = 2\times10^{-5}$ K^{-1}. If the tensile strength is taken to be in the range 10–100 MPa, then the value of ΔT required for fracture formation is calculated in the range 17–170°C. If the strength of the crust is low (10 MPa), perhaps due to the existence of flaws, then small-scale fractures should develop almost immediately after the surface cools much below 600°C. However, a strong crust (100 MPa) would be expected to start fracturing when the surface temperature had declined below about 430°C. Our cooling model indicates that this would start to happen after slightly over an hour and the elastic part of the crust (defined by the 600°C isotherm) would be at about 1.5 cm thick. This result is consistent with the observation that the smallest scale fracture widths at the surface are about 1 cm (Figs. 3 and 12b), on the assumption that fracture width and depth of the fractured layer are comparable. If glass strength is comparable to the strongest natural glasses at about 300 MPa (Dingwell, 1998) then the surface might have to cool to almost ambient temperature before fracturing occurred. It is even feasible that stresses are never quite large enough for fracturing. Indeed, the small-scale joint network is patchily developed, suggesting that in places the crust has considerable strength. K. Hon (personal communication) has observed that similar polygonal joint networks develop on pahoehoe lava surfaces in Hawaii several hours to weeks after emplacement. We conclude that the stored tensile stresses in the crust resulted in local development of the polygonal network, particularly in areas where crustal flexure added additional tensile stresses.

8. Conclusions

We now summarize our interpretation of the evolution of the Tenerife crust and its fracture system.

1. After emerging from the lava tube, the lava spread rapidly as a pahoehoe sheet flow, filling the local depression within a few minutes. The crust began to consolidate and gas bubbles began to rise through the lava interior. The bubbles started to accumulate beneath the growing lava crust, causing slow inflation of the lava in these first few hours.
2. For unknown reasons, the gas accumulation varied laterally with centres of gas accumulation developing at spacing of several metres to create local buoyant forces. Uplift developed progressively over about 2 h by which time the crust (defined at the 950°C isotherm) was about 10 cm thick. During this time, tensile stresses accumulated in a much thinner elastic zone due to thermal contraction and crustal flexure.
3. Two different estimates of the thickness of the elastic zone are based on the relaxation time of the residual glass and on the observed bending of the slabs using theory for a plate with a central force. They both give a thickness of about 2 cm for when the slabs rifted apart.
4. We attribute the formation of the large-scale slab-bounding fractures to tensile stresses due to uplift of the slab centres. Flow parallel fractures developed earlier, indicating that residual down-slope stresses or lava flow also had influence.
5. During flexural bending of the slabs, an intermediate

rectilinear scale (25 cm) of fractures developed with most joints parallel to the orthogonal slab-bounding fractures. The elastic zone of the crust was increasingly stressed towards the surface due to cooling contraction. Thus a network of small-scale (6 cm) joints developed, which locally perturbed the propagation of both the intermediate and large-scale fracture networks. The development of the small-scale polygonal joint network is particularly strong at the slab edges, where the bending tensional stresses added to cooling-related stresses.

6. Lava crusts are concluded to be weak. Lava movement is inhibited by the growth of a crust. However the behaviour of lava crust is dependent on strain rate as well as temperature. For glassy lava crusts, the elastic zone of the crust is quite thin in comparison to the depth of lava that is affected by cooling. The elastic zone is a region where thermo-elastic tensile stresses due to cooling and stretching can increase and attain the strength of the crust at the outside. Fractures originating at the surface can however penetrate deep into the plastic zone. A highly fractured elastic crust can have no strength in tension.

Acknowledgements

Michelle Dance and Andrew Wallman acknowledge NERC and EPSRC studentships, respectively. RSJS acknowledges EC grant (EV SV-CT93-0283), the Leverhulme Trust (F/182/A1) and a NERC Research Professorship. The authors would like to pay tribute to our late colleague Paul Hancock. His incisive observations and expertise on fracture architecture were invaluable contributions to this study, as was his congenial company in the field. The content and organisation of this paper were substantially improved by penetrating and detailed reviews by Ken Hon, Attila Aydin, Kathy Cashman, Terry Engelder and Bill Dunne.

Appendix A. Thermal modelling

The one-dimensional model is shown in Fig. 15. Temperatures are scaled relative to the fusion temperature T_f, lengths are given in units of $(\varepsilon\sigma T_f^3)/k$ and the following re-scalings are used in the subsequent analysis:

$$t' = \frac{\left(\varepsilon\sigma T_f^3\right)^2}{\rho C_p k} t, \nu = \frac{T_a}{T_f}, \qquad \theta(t') = \frac{V(t)}{T_f},$$
$$\Re = \frac{h}{\varepsilon\sigma T_f^{8/3}}, \qquad \alpha = \frac{L}{C_p(T_f - T_a)}, \tag{A1}$$

Thus the problem is reduced to a dimensionless form with notation as defined in Table A1. In the subsequent presentation, the prime notation is dropped for clarity. Heat transfer is taken to occur by conduction alone, and so the problem reduces to the classical one-dimensional diffusion equation in the central region of the ponded lava,

$$\frac{\partial T_s}{\partial t} = \frac{\partial^2 T_s}{\partial x^2}, \qquad x \in (0,\ s(t)) \qquad \text{and} \qquad t > 0 \tag{A2}$$

Quantifying the combined effects of heat loss at the free surface due to radiation and turbulent, natural convection requires that

$$\frac{\partial T_s}{\partial x} = \left(T_s^4 - v^4\right) + \Re(T_s - v)^{4/3} \qquad \text{on} \qquad x = 0, \tag{A3}$$

where the convective heat transfer coefficient h, in the dimensionless parameter $\Re$ is given empirically by Chu and Goldstein (1973) from experimental measurements. The Stefan condition at the phase boundary simply states that the release of latent heat must match the local difference in heat flux at the boundary. As this boundary is defined as the melt temperature then these two conditions require that:

$$T_s = 1 \qquad \text{and} \qquad \frac{\partial T_s}{\partial x} = \alpha\frac{ds}{dt} \qquad \text{on} \qquad x = s(t) \tag{A4}$$

As the lava is initially emplaced at its initial temperature, then the initial conditions to complete the statement of this problem are

$$T_s = 1 \qquad \text{when} \qquad t = 0\ \forall\ x > 0 \tag{A5}$$

A technique proposed by Goodman (1958) arising from boundary layer theory, is applied. This technique assumes the spatial form of the isotherms thus reducing the number

Table A1
Notation used in Appendix A

Parameter	Symbol	Unit
Atmospheric temperature	T_a	K
Coefficient of thermal expansion	α	
Convective heat transfer coefficient	h	$Wm^{-2}K^{-4/3}$
Co-ordinate direction	x	Dimensionless
Emissivity	ε	Dimensionless
Fusion temperature	T_f	K
Latent heat	L	Jkg^{-1}
Poisson's ratio	U	Dimensionless
Proportion of vesicles	θ	Dimensionless
Ratio of background to fusion temperature ($=T_a/T_f$)	ν	Dimensionless
Ratio of convective to radiative heat fluxes ($=h/(\varepsilon\sigma T_s^{8/3})$)	$\Re$	Dimensionless
Solid conductivity	k	$Wm^{-1}K^{-1}$
Solid density	ρ_s	kgm^{-1}
Solidification front distance	$S(t)$	Dimensionless
Solid temperature	T_s	Dimensionless
Specific heat capacity	C_p	$Jkg^{-1}K^{-1}$
Stefan-Boltzmann constant	σ	$Wm^{-2}K^4$
Stefan number ($=L/C_p(T_f - T_a)$	α	Dimensionless
Surface temperature	θ_t	Dimensionless
Surface temperature	V_t	K
Tensile strength	σ_T	Pa
Time scale	t	Dimensionless
Young's Modulus	E	Dimensionless

of independent variables involved in the problem. Eq. (A4) thus reduces to a temporal ordinary differential equation (ODE) which can be solved using standard numerical schemes. Assuming a quadratic form for the isotherm structure and enforcing the boundary conditions (A3)–(A4) reduces this statement of the problem to,

$$\frac{2(1-\theta)}{s} - 2\left(\theta^4 - v^4\right) - 2\Re(\theta - v)^{4/3} = \frac{2}{3}s\frac{\mathrm{d}\theta}{\mathrm{d}t}\left(1 + s\theta^3 + \frac{\Re s}{3}(\theta - v)^{1/3}\right) + \frac{s}{3}\frac{\mathrm{d}s}{\mathrm{d}t}\left(\left(\theta^4 - v^4\right) + \Re(\theta - v)^{4/3} - \frac{2(1-\theta)}{s}\right) \quad \text{(A6)}$$

$$\frac{2(1-\theta)}{s} = \left(\theta^4 - v^4\right) + \Re(\theta - v)^{4/3} + \alpha\frac{\mathrm{d}s}{\mathrm{d}t} \quad \text{(A7)}$$

with the initial conditions requiring that $s(0) = 0$ and $\theta(0) = 1$. The initial indeterminacy becomes clear once the problem is posed in this form. This problem can now be overcome from the derivation of a small-time asymptotic solution to give Eqs. (A5) and (A6). Posing a temporal Poincaré expansion for the interface motion and the surface temperature, and solving at successive orders yields

$$\theta(t) = 1 - \frac{t}{\alpha}(v - 1) \times\left(v^3 + v^2 + v + \sqrt[3]{(1-v)}\Re + 1\right)^2 + O\left(t^2\right) \quad \text{(A8)}$$

for $t \ll 1$

$$s(t) = \frac{t}{\alpha}(v - 1)\left(v^3 + v^2 + v + \sqrt[3]{(1-v)}\Re + 1\right)^2 + O\left(t^2\right)$$

for $t \ll 1$ (A9)

these equations are used to start the numerical scheme. A standard numerical scheme from the N.A.G. libraries, employing an Adams–Moulton method (Gear, 1971), was used to solve the coupled system of ODEs (A6)–(A7) by starting the scheme using Eqs. (A8) and (A9).

Bubbles modify heat transfer since they alter the thermal conductivity of the lava and introduce cavities with the potential for convective and radiative heat transport (Keszthelyi, 1994). Keszthelyi (1994) found that larger bubbles, of average dimension greater than 1 cm, permit radiation and convection across their interior. Whilst in smaller vesicles, heat transfer occurs solely by conduction across the gas pockets and convection is suppressed even when large temperature gradients exist in the melt ($\sim$1000 K cm^{-1}). The vesicles in the Tenerife lava have an average diameter of 3 mm, excepting the sheared bubbles at the very surface, indicating that heat transfer is only by conduction. Internal heat transfer is therefore taken to occur predominantly by conduction across the vesicles. This is incorporated by using proportionally modified values for the conductivity k, the sensible heat content ρC_p and the latent heat of fusion L, using, for example,

$$k_{\text{overall}} = (1 - \varnothing)k_{\text{lava}} + \varnothing k_{\text{gas}} \qquad 0 < \varnothing < 1 \qquad \text{(A10)}$$

where $\varnothing$ here represents the proportion of vesicles.

References

Ablay, G., Carroll, M.R., Palmer, M.R., Marti, J., Sparks, R.S.J., 1998. Basanite–phonolite lineages of the Teide–Pico Viejo Volcanic Complex, Tenerife, Canary Islands. Journal of Petrology 39, 905–936.

Anderson, O.L., Grew, P.C., 1977. Stress corrosion theory of crack propagation with applications to geophysics. Review of Geophysics and Space Physics 15, 77–104.

Budkewitsch, P., Robin, P.Y., 1994. Modelling of the evolution of columnar joints. Journal of Volcanology and Geothermal Research 59, 219–239.

Chu, T.Y., Goldstein, R.J., 1973. Turbulent, natural convection in a horizontal layer of water. Journal of Fluid Mechanics 60, 141–159.

De Graff, J.M., Aydin, A., 1993. Effect of thermal regime on growth increment and spacing of contraction joints in basaltic lava. Journal of Geophysical Research 98, 6411–6430.

Dingwell, D.B. 1998. Recent experimental progress in the physical description of silicic magma relevant to explosive volcanism. In: Gilbert and Sparks, R.S.J. (Eds), The Physics of Explosive Volcanic Eruptions. Geological Society, London, Special Publication 145, 9–26.

Dingwell, D.B., Webb, S.L., 1989. Structural relaxation in silicate melts and non-newtonian melt rheology in igneous processes. Physics and Chemistry of Minerals 16, 508–516.

Gear, C.W., 1971. Numerical initial value problems in ordinary differential equations. Prentice-Hall, Englewood Cliffs.

Goodman, T.R., 1958. Heat-balance integral and its application to problems involving a change of phase. ASME Transactions C 80, 335–342.

Hancock, P.L., 1985. Brittle microtectonics: principles and practice. Journal of Structural Geology 7, 437–457.

Hearns, E.J., 1989. Mechanics of Materials. Volume 2. International Series on Materials Science and Technology 19, 431–905.

Hon, K, Kauahikuaa, J., Denlinger, R., Mackay, K., 1994. Emplacement and inflation of pahoehoe sheet flows: observations and measurments of active lava flows on Kilauea volcano, Hawaii. Geological Society of America Bulletin 106, 351–370.

Keszthelyi, L, 1994. Calculated effect of vesicles on the thermal properties of cooling basaltic flows. Journal of Volcanology and Geothermal Research 63, 257–266.

Murase, T., McBirney, A.R., 1973. Properties of some common igneous rocks and their melts at high temperatures. Geological Society of America Bulletin 84, 3563–3592.

Neuville, D.R., Courtial, P., Dingwell, D.B., Richet, P., 1993. Thermodynamic and rheological properties of rhyolite and andesite melts. Contributions to Mineralogy and Petrology 113, 572–581.

Peck, D.L., 1978. Cooling and vesiculation of Alae lava lake, Hawaii. U.S. Geological Survey Professional Paper 935-B, 1–59.

Peck, D.L., Minakami, T., 1968. The formation of columnar joints in the upper part of Kilauean lava lakes, Hawaii. Geological Society of America Bulletin 79, 697–704.

Pinkerton, H., Sparks, R.S.J., 1976. The 1975 Sub-terminal Lavas, Mount Etna: A Case History of the Formation of a Compound Lava Field. Journal of Volcanology and Geothermal Research 1, 167–182.

Provost, A., Bottinga, Y., 1972. Rates of Solidification of Apollo II Basalt and Hawaiian Tholeiite. Earth and Planetary Science Letters 15, 325–337.

Röedder, P.L., Emslie, R.F., 1970. Olivine–liquid equilibrium. Contributions to Mineralogy and Petrology 29, 275–289.

Ryan, M.P., Belvins, J.Y.K., 1987. The viscosity of synthetic and natural silicate melts and glasses at high temperature and 1 bar (105 Pascals)

pressure and at higher pressures. U.S. Geological Survey Bulletin 1764, 563.

Walker, G.P.L., 1991. Structure and origin by injection under surface crust of tumuli, “lava rise”, “lava rise pits”, and “inflation clefts” in Hawaii. Bulletin of Volcanology 53, 546–558.

Worster, M.G., Huppert, H.E., Sparks, R.S.J., 1990. Convection and crystallisation in magma cooled from above. Earth and Planetary Science Letters 101, 78–89.